International Journal of Engineering

Journal Homepage: www.ije.ir

Experimental Study for Investigating the Mechanism of Heat Transfer Near the Critical Heat Flux in Nucleate Pool Boiling

B. S. Sikarwar*, R .K. Shukla, S. K. Sharma

Amity School of Engineering Technology, Amity University Noida (UP), India

P A P E R I N F O

Paper history:
Received 15 April 2015
Received in revised form 05 June 2015
Accepted 12 June 2015

Keywords:
Pool Boiling Nucleate
Macro-layer
Mashroom
Critical Heat Flux
Vapor Mass
Frequency

A B S T R A C T

The regime of nucleate pool boiling near critical heat flux (60-98% of CHF) is known as vapor mushroom regime. Understanding the mechanism of heat transfer in regime of vapor mushroom of nucleate pool boiling is not only helpful to explain high rate heat transfer, but also useful to explain boiling crisis phenomenon. In this paper, an experimental setup is designed and fabricated to study the mechanism of heat transfer from boiling surface to bulk liquid near critical heat flux (vapor mushroom regime). In addition, vapor mass frequency and thickness of macro-layer are measured at various heat fluxes in this regime of boiling. The experimental study reveals that individual bubbles coalesce due to very high bubble site density and form vapor mass entrapping a relatively thicker film of liquid known as 'macro-layer' between the growing vapor mass and the heating surface of pool boiling near the high heat flux region. The rate of evaporation of macro-layer and transient conduction through macro-layer is the prime parameter to transfer heat from the heated surface. The thickness of the macro-layer is found to be lying in the range of 153- 88 μm, respectively, for range of 60-98% critical heat flux. As the heat flux increases, the thickness of macro-layer decreases. The vapor mass frequency varies from 4 to 8.80 Hz for water in the range of 60-98 % of critical heat flux. The vapor mass frequency increases as heat flux increases due to higher evaporation rate associated with higher heat flux. The data reported in this manuscript are more consistent as comparing to data available in the literature and these data are useful in modeling heat transfer in nucleate pool boiling near critical heat flux.

***doi**: 10.5829/idosi.ije.2015.28.08b.18*

1. INTRODUCTION

Boiling heat transfer has always been a subject of interest for scientists and engineers alike, because of the ability of the mechanism to extract heat from any system at very high rates and also due to the fact that even after nine decades since it was first investigated, there are so many possibilities and variables that have not been fully explored [1-3]. In any kind of boiling behavior, several factors like surface tension, buoyancy, surface roughness, operating temperature and pressure, interaction of bubbles with each other, etc. simultaneously come into play [4-7]. Predicting the behavior of such a system is a very challenging task; although it is complex phenomena but it is one of the most efficient modes of heat transfer and finds its applications in areas such as electronic device cooling, refrigeration, air conditioning power generation, chemical processing, nuclear reactors, rocket motors and any phase process where quick removal of heat energy from a hot surface is desired [8-10].

Gaertner [11] conducted a photographic study of nucleate pool boiling of water at atmospheric pressure on 2/0 polished platinum and 4/0 polished copper horizontal surfaces and classified the typical nucleate boiling regimes on a classical boiling curve of heat flux versus wall superheat. These are incipient boiling, discrete bubble region, first transition region, vapor mushroom region, second transition region and critical heat flux (CHF) point. Figure 1 shows the formation of vapor structured in nucleate pool boiling in different regimes of pool boiling. Bhat et al., [12, 13] further subdivided the Gartner's second transition region into

*Corresponding Author's Email: bssikarwar@amity.edu (B. S. Sikarwar)

Please cite this article as: B. S. Sikarwar, R .K. Shukla, S. K. Sharma, Experimental Study for Investigating the Mechanism of Heat Transfer near the Critical Heat Flux in Nucleate Pool Boiling, International Journal of Engineering (IJE), TRANSACTIONS B: Applications Vol. 28, No. 8, (August 2015) 1241-1250

two sub-regions; (i) second transition interface region and (ii) macrolayer region. They suggested that the interference region lies between 0.17 and 0.5 q_c and the macro-layer region lies between 0.6 and q_c. The regime of this range of heat flux (0.6 and q_c) is called vapor mushroom regime. In this regime of boiling, the individual bubbles coalesce due to very high site bubble density and form vapor masses entrapping a relative thicker film of liquid known as macro-layer between the growing vapor mass and heating surface, as shown in Figure 2. Kirby and Westwater [14] photographed the phenomenon of nucleate boiling through a transparent boiling surface with carbon tetrachloride and methanol as the boiling fluids. They identified three general type of bubbles, which were called type I, type II, and type III bubbles. Their research concluded that the mechanism of nucleate pool boiling is very complicated and there was not agreement on the details of just how nucleate boiling actually accomplishes the transfer of heat.

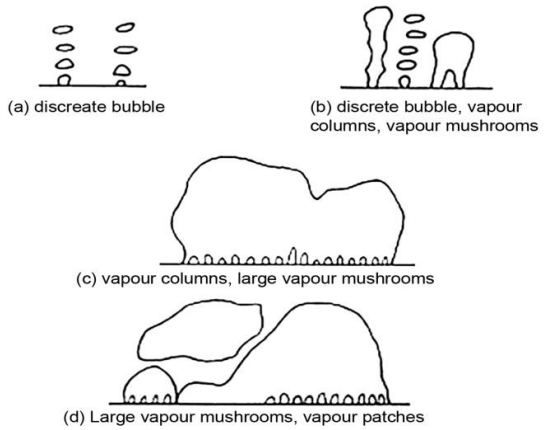

Figure 1. Sketch of vapor structure observed in nucleate pool boiling of water from a flat horizontal surface by Gaertner [11]. (a) Discrete bubble region, (b) first transition region, (c) vapor mushroom region and (d) second transition region.

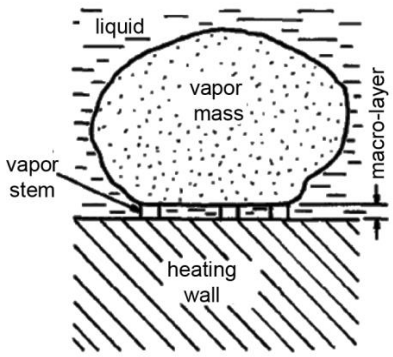

Figure 2. Mechanism of heat transfer in nucleate pool boiling under high heat flux [13]

For vapor mushroom regimes of nucleate boiling, many researchers [15-19] supported the existence of the macro-layer immediately adjacent to the heated surface. This liquid layer is distinguished from the micro-layer that exists under the base of individual nucleating bubbles. They noted that the macro-layer contains numerous columns or stems of vapor, as shown in Figure 2. At short distances from the heater, they found that vapor stems from several adjacent active nucleation sites merged into a large vapor mushroom. The occurrence of CHF has been linked closely to the behavior of the macro-layer. Gaertner [11] proposed that CHF occurred as a result of the collapse of the vapor stems because of hydrodynamic instabilities on their walls. He conjectured that such a collapse of the stems causes the formation of dry patches on the heated surface. In his opinion, classical Kelvin–Helmholtz instabilities may not be applicable in this situation because the predicted values were orders of magnitude higher than the thickness of the liquid layer observed by Kirby and Westwater [14]. Additionally, Sadasivan et al. [20] postulated that Kelvin–Helmholtz instabilities do not appear to be the main factor in determining the macro-layer thickness. The macro-layer formation mechanism has been examined based on available detailed experimental measurements of vapor and liquid flow patterns close to the heated surface. Katto and Yokoya [21] proposed that CHF was the result of consumption of the macro-layer due to evaporation. They noted that the supply of liquid to the heater surface occurs only when the vapor mushroom detaches from the macro-layer. Immediately after the mushroom departs, fresh liquid is supplied to the heated surface, the macro-layer is reestablished, and a new vapor mushroom begins to grow above it. The time period between the inception and departure of the mushroom is termed the hovering period of the mushroom. Thus, they postulated that the heater surface becomes completely dry when the time required to evaporate the entire macro-layer is less than the hovering period of the vapor mushroom. Bhat et al. [22] reported that the thickness of the liquid layer between the heated surface and the vapor mass has a linear relationship with the diameter of vapor stems.

A lot of researchers [16, 18, 23-27] observed that near critical heat flux macro-layer plays a key role in heat transfer. Noteworthy, a good number of analytical models and numerical simulations for boiling heat transfer were based on the concepts of near-wall micro-layer and macro-layer whose thicknesses were estimated to range from several μm to some hundreds μm. However, an experimental quantification of the behavior of such thin liquid films is not straightforward, since the measurement at micro scale is a challenge, and further complicated by the traditional experimental setups (e.g. pool boiling with heater block) and the

chaotic nature of boiling process which impede direct/camera observation and measurement of the thin liquid films, especially under high heat flux conditions. Very few researchers [13, 27] reported data of the initial thickness of macro-layer and vapor mass frequency. But, these data are inconsistent and incompetent for very small range of heat flux. Although boiling has been studied broadly during the last five decades which includes experimental work and theoretical models, prediction of exact nature of boiling in various heat flux conditions near critical heat flux is uncertain. Since the boiling process near critical process is very complex, its complete understanding still poses significant challenges.

Against this background, we have designed and fabricated experimental setup which not only serves for visualizing the boiling phenomenon, but also measures the frequency of vapor mass and initial macro-layer thickness. In this paper, we describe a macro-layer formation along with variation of initial macro-layer thickness and vapor mass frequency at various heat fluxes in vapor mushroom regime of water boiling on brass surface at atmospheric pressure.

2. EXPERIMENTAL SETUP

The photograph of experimental setup for investigating the mechanism of pool boiling under high heat flux is shown in Figure 3(a) and (b) which properly illustrates the labelled schematic diagram of the setup. The major components of the setup are the heater assembly, boiler vessel, condenser, electrical resistance probe, data logger system and a high speed camera. The heat energy was generated by heater that was embedded at the bottom of the boiling surface in bulky brass block. The heating element at the bottom of this brass block was embedded during casting of this block. The boiling took place inside the boiler vessel and vapor was condensed in the condenser and finally condensate was returned back to the boiler vessel by gravity. The heat flux was changed using an adjustable auto transformer. A conductance-based probe, inserted into the boiler vessel from its top, was traversed in the space close to the boiling surface with the help of a micrometer fitted at the top of the probe. The whole assembly was leak proof. Level indicator was provided to indicate liquid level in the vessel, as shown in Figure 3. Pressure and air relief valves were provided at the top of the vessel for measuring pressure of vessel and removal of air from the vessel if required. Condenser was fitted inside the boiler vessel at top side and bottom side, heating the assembly with heating arrangement.

The heater assembly, as shown in Figure 4, was fabricated of brass material by casting method. It includes two parts (i) heating element assembly, (bottom side of assembly) and (ii) heat conductor with boiling surface assembly (top side of assembly). The whole assembly was casted in one piece so as to minimize heat loss and save material, energy and space. The components of this assembly (heating element and heat conductor with boiling surface) were identified by their diameters. The bottom side heater assembly was 60 mm diameter and 60 mm long cylindrical brass block. Nicrome (diameter 2 mm) wires were embedded during the casting of this assembly. To supply power to the heating element, two terminals were provided at the bottom of the assembly, as shown in Figure 4. The power was supplied to it through an adjustable auto transformer and a voltage stabilizer.

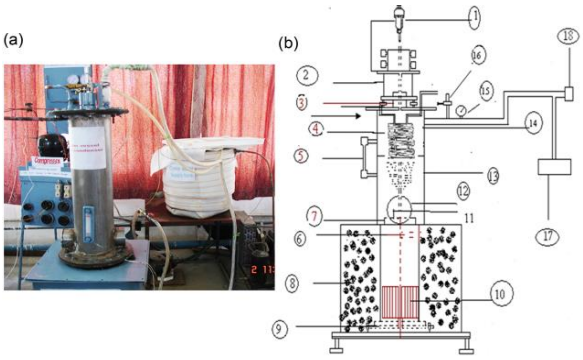

Figure 3. (a) Photograph of experimental setup. (b) Schematic diagram of experimental setup with accessories. The accessories are: (1) micrometer, (2) probe holder, (3) pressure seal, (4) electrical resistance probe, (5) liquid level indicator, (6) thermocouples, (7) boiling surface, (8) glass wool, (9) electrical insulation, (10) heating rods, (11) teflon ring, (12) glass windows, (13) boiler vessel, (14) condenser, (15) Pressure gauge, (16) air vent, (17) refrigerant charging kit and (18) vacuum pump.

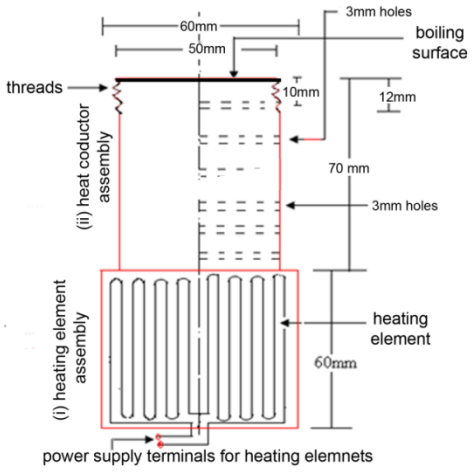

Figure 4. Heater assembly with its components. (i) Heating element assembly, (ii) heat conductor assembly and (iii) boiling surface.

The maximum capacity of the heater element is 4.5±0.5 kW. The corresponding maximum flux to provide the boiling surface is approximately 2MW/m^2. The bulky block was placed on a mild steel stand with thick asbestos sheets kept between the block and stand to prevent heat loss. The heater stand and box were provided with leveling screws to keep the axis of the block in vertical position so that boiling surface was perfectly horizontal.

The cylindrical block of brass with 50 mm diameter and 80 mm length was heat conductor assembly. The top surface of it was used as boiling surface. The threads were cut at top side of the brass conductor for hooking up the heater assembly with boiler vessel. A Teflon ring that had internal and external threads was used to connect the heater assembly to the boiler vessel. In this way, the Teflon ring acted as a sealant for liquid in the boiling vessel and also prevented heat loss from the conductor to vessel.

The top surface of the conductor used as the boiling surface was polished with a 4/0 grade emery paper. Six holes of 2 mm diameter were drilled in the brass conductor up to center of the conductor. These holes were placed at equal interval of 10 mm in the axial direction as shown in Figure 4. In these holes, ceramic tubes were inserted so that the thermocouple beads were in contact with the conductor surface along the central axis of the conductor. The brass conductor received uniform heat flux at bottom from the block. Two chromel-constantan thermocouple of 30 standard wire gauge (SWG) were fitted in each hole to measure temperature along the axis of the conductor. Extra precaution was taken to ensure that the thermocouple beads were in contact with the conductor surface along the central axis of the conductor.

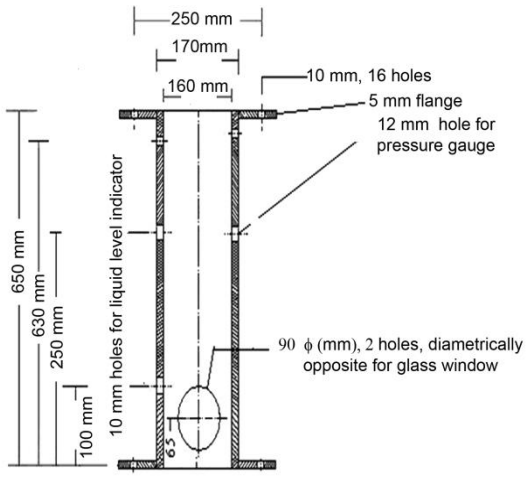

Figure 5. Cross-sectional view of boiler vessel with various holes for fitting accessories with dimensions and position of holes.

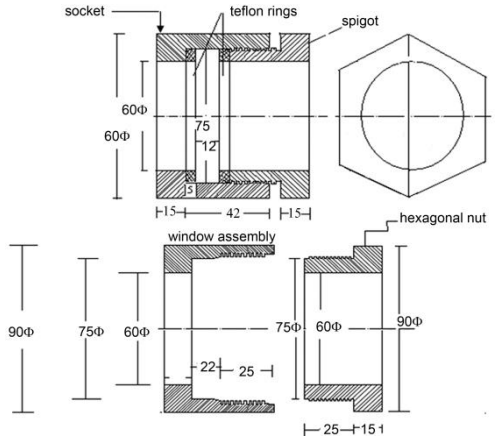

Figure 6. Complete drawing of glass windows with dimensions.

Figure 5 shows cross section view of boiler vessel. A seamless stainless steel pipe having inner diameter of 160 mm, outer diameter 170 mm and length 650 mm was used for fabrication. Stainless steel flanges with twelve holes each (Figure 5) were welded at top and bottom end of the vessel. At 65 mm from the bottom flange, two glass windows diametrically opposite to each other were provided in the vessel for visualizing the boiling phenomenon on boiling surface. Two holes of 10 mm diameter each were drilled at 100 mm and 300 mm on the vessel above bottom flange as shown in Figure (5) for fitting a liquid level indicator on the vessel for visual observation of liquid level in the vessel. The flange welded at top of the vessel could be closed by the cover plate tightened to it by nuts and bolts with a thick neoprene packing between the mating surfaces. A central hole drilled in the cover plate was used for inserting an electrical resistance probe and another hole for inserting a thermocouple used for measuring the bulk liquid temperature. The dimensions and assembly of glass windows is shown in Figure 6. They had socket which was welded on the vessel around opening window of the vessel. A Pyrex glass 75 mm in diameter was fitted inside the socket with two Teflon rings and asbestos packing with O-ring on the two sides. The end of the spigot is made in the shape of the hexagonal nut to facilitate tightening, as shown in Figure 6.

A mica sheet was wrapped around the boiler vessel and a nicrome wire in fiber glass sleeve was coiled over it. This coil was then covered with asbestos rope and a thick coating of plaster of Paris. This arrangement helped in effectively preventing the major portion of heat losses through the boiler vessel. A vertical 1 kw immersion heater was inserted through the cover plate to provide required energy for marinating the liquid at the saturation temperature. The steam pipe (copper) was provided with its usual fittings like safety valve,

pressure gauge and air vent valve. Condenser was fitted inside and top of the vessel. Cooling water inlet and outlet pipes were provided for continuous supply of cold water in condenser coil. A thick insulation comprising of asbestos rope and coating of plaster of Paris was provided over these pipes to prevent the heat losses. It was found that if the power input to the brass block was increased through large steps, film boiling could occur prematurely. Due to this, high heat flux values were approached by increasing power input slowly and gradually. A number of runs were repeated to check the reproducibility which was found to be satisfactory. On attaining steady state, the liquid was permitted to boil for about 2 hours before recording the data. The high thermal capacity of the copper block saved the equipment from overheating and burning out. The only damage that occurred during the film boiling was overheating of the Teflon ring in contact with the copper conductor which had to be replaced.

3. EXPERIMENTAL PROCEDURE

The apparatus leakage was tested under high pressure using compressed air. All the electrical circuits were checked for continuity. The thermal conductivity of conductor material was measured. It was 108±5 W/m K. The thermocouples were calibrated. The apparatus was leveled with respect to the horizontal surface so that the boiling surface was horizontal and probe was in vertical position. The power was supplied to the heater through a 10 KVA oil- cooled automatic voltage stabilizer with variac. As mentioned earlier, the boiling surface was prepared to the desired specification of smoothness using a 4/0 grade emery paper. The boiler vessel was filled with about 4.5 liters of DI water (levels were checked by liquid level indicator). The probe tip was cleaned and the vessel was closed with the cover plate. The probe assembly and the thermocouples were attached. Power supply to all the heating elements was then switched on. The power input to the heater elements was adjusted to some initial values by the 10 KVA adjustable auto transformer. The cooling water supply was then opened to circulate cooling water in the condenser. Energy inputs to the heater elements were gradually increased to the required heat flux level. At low heat flux, increments of comparatively large magnitude could be given whereas in the high heat flux region, increments were very small to avoid the sudden occurrence of film boiling. Under low heat flux conditions, an increment of about 5% of supply voltage was given while under high heat flux condition, it was reduced to about 2% of supply voltage. After each increment, half an hour time was allowed for temperatures to reach the steady state value. Thermocouple readings were recorded throughout the day corresponding to each increment in input voltage. When the final steady state reached the desired heat flux, the thermocouple readings were recorded.

The schematic diagram for temperature measurement is shown in Figure 7. Twelve chromel-constantan (E type) thermocouples were fitted in the brass conductor to measure the temperature along the axis. These thermocouples had temperature range of -173K to 1273K. The thermocouples were duly calibrated before fixing in the conductor. Two thermocouples were located at one place to ensure the better accuracy of temperature measurement at given place. It means at six places, twelve thermocouples were located. Lab View 5.1 was used for measuring temperature of brass conductor. The thermocouples fixed in brass conductor at location, as shown in Figure 7, were connected to the terminal box of data logger system through extension wire. Terminal box (SCXI 1303, 32 channels) was connected to module (SCXI 1102) and DAQ card in CPU of PC. G Programming for writing code was used in Lab view for measurement of the temperature of conductor.

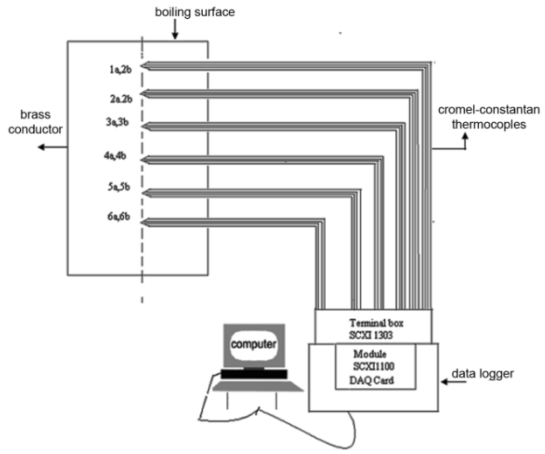

Figure 7. Schematic diagram for the temperature measurement of heater and boiling surface using thermocouples.

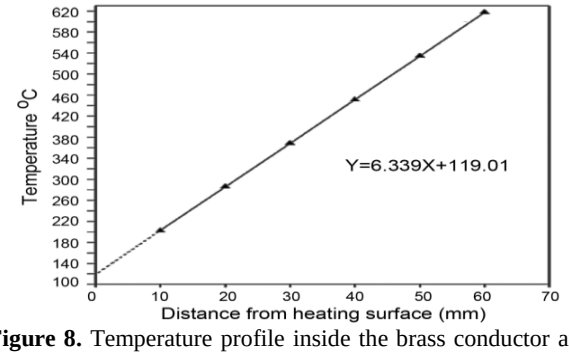

Figure 8. Temperature profile inside the brass conductor and procedure for determination of the temperature of the surface by linear extrapolation.

By knowing the temperature profiles in brass conductor, the boiling surface temperature was determined from the extrapolation of the temperature versus distance, as shown in Figure 8. The saturation temperature of boiling liquid was determined using a thermocouple suspended about 20 mm and 45 mm above boiling surface. The wall heat flux was calculated using Fourier's law for steady state conduction in copper conductor as:

$$q = -k\left(\frac{dT}{dX}\right)_{x=0} \quad (1)$$

where, k is the thermal conductivity of brass (108 W/m K) and $(dT/dx)_{x=0}$ is the temperature gradient at the boiling surface.

The axial temperature plot obtained for a typical case of water at run no. 16 from the extrapolation of the temperature profile was found to be 119.01 ^{o}C, and the corresponding wall heat flux calculated from Equation (1) was 0.904x106 W/m^2. Observing the best fit straight line for temperature profile (i.e. y=8.339x+ 119.01), the interception gives the surface temperature as 119.0 ^{o}C. Similarly, surface temperature measurement for other run no. (Heat flux) was estimated.

Line diagram for measuring bubble frequency and vapor mass emission frequency using electrical resistance probe and digital storage oscilloscope is shown in Figure 9(a). It works on the principle of electrical conductivity difference of the water and water vapor. Therefore, this method is called conductance base probe method. The detecting component consists of electrical resistance probe with an exposed tiny electrode projecting into the liquid and plate electrode which is so large that the liquid is always in contact with it. The tip of the probe wire with a diameter of 0.1 mm was considered as the tiny electrode while the heating surface having a diameter of 50 mm was considered to be the large electrode. The electrical resistance between these electrodes is determined by whether the tiny electrode is dipped in the liquid or vapor phase. Consequently the voltage fluctuation across the probe tip and heating surface gap is higher when the tip is in contact with vapor. The conductance of the medium within the gap between the probe tip and heating surface decreases whenever a bubble or vapor mass strikes the tip of the probe wire and thus the output voltage signal decreases intermittently. Direct current (DC) was supplied in the circuit by the two 12 V batteries.

The power supply to the oscilloscope and the D.C. supply to the probe circuit were switched on. The probe was pushed downwards so as to make an electrical contact of the probe tip with the boiling surface. The micrometer readings corresponding to this position indicate the initial reading of micrometer. The probe is then lifted to a height of 3 mm above the boiling surface. The probe was now set for taking the frequency measurement using the oscilloscope. Micro displacements were given to the probe in the downward direction and the micrometer reading and the frequency was recorded at each position during its downward travel. The galvanometer gives a sudden deflection when the probe tip touched the boiling surface which signaled the completion of a set of observations. The heat flux is increased and similarly reading is recorded after the steady state corresponding to new heat flux. The wall heat flux, wall superheat, initial macrolayer thickness and vapor mass frequency data are recorded for the water. The sweep on the oscilloscope screen was held at any instant and the numbers of voltage fluctuations were counted. The bubble or vapor mass frequency was determined by dividing the number of voltage fluctuations by the total sweep time at that instant. For each voltage fluctuation, the oscilloscope beam represents a bubble or vapor mass emitted at that time and consequently the number of voltage fluctuation observed on the oscilloscope screen over a fixed time interval can be interpreted as the bubble/ vapor mass frequency. Since the bubble/vapor mass frequency is of random nature, five readings of the signal at each point were taken and averaged to obtain the bubble/vapor mass frequency at that point. Figure 9(b) shows photograph of probe during experiment.

4. RESULTS AND DISCUSSION

The experimental setup, described in previous section, was used for measuring wall heat flux, initial macro-layer thickness and vapor mass frequency at various degrees of superheat of water boiling on brass surface near the high heat flux. This data is very useful in modeling of nucleat,e specifically near critical heat flux.

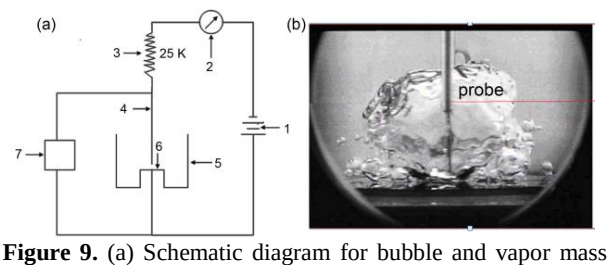

Figure 9. (a) Schematic diagram for bubble and vapor mass frequency measurement and initial macro-layer thickness. The components are: (1) 24 V batteries, (2) galvanometer, (3) fixed resistances, (4) electrical resistance probe, (5) boiler vessel, (6) boiling surface and (7) digital storage oscilloscope. (b) Photograph of vapor mass growing and procedures of measurement of macro-layer thickness using probe.

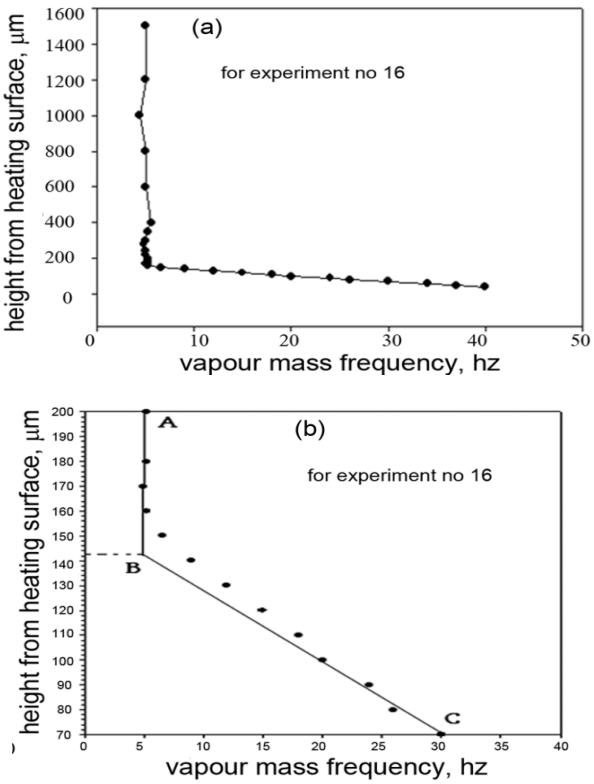

Figure 10. Method for determining the macro-layer thickness. Figure (a) shows the variation of vapor mass frequency with respect to the height from the heating surface and Figure (b) shows the in-large view of this variation. Both figures show methodology of determining the macro-layer thickness at heat flux =0.98MW/m^2 (Run16) of water boiling on brass surface.

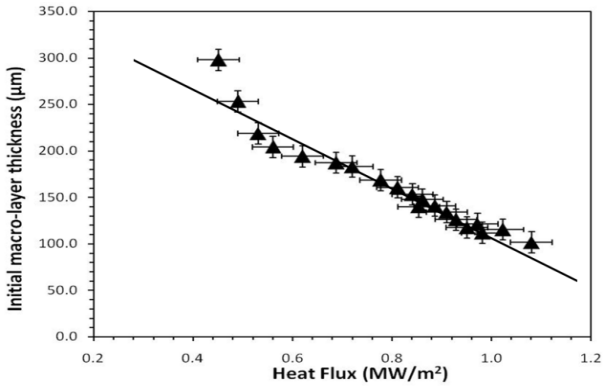

Figure 11. Variation of initial macro-layer thicknesses (µm) with respect to heat flux (MW/m^2). Distilled water was boiled on brass surface at room temperature (32 ^{o}C) and pressure is equal to one atm. The critical point for this boiling surface is $\approx$1.15 MW/m^2.

Figure 10 shows the procedure of measuring macrolayer thickness and vapor mass frequency for run no 16 (input heat flux =0.98MW/m^2). As the macrolayer is very thin and its thickness varies both with time as well as spatially, direct measurement of its thickness is not possible. Therefore, the conductance probe method (described above) was used to measure macrolayer thickness and vapor mass frequency. Figure 10 shows that the vapor mass frequency is constant; it is represented by the vertical line AB at given heat flux (run 16). When the probe is pushed to a point very close to the heating surface, it enters the macro-layer region. It was estimated that average distance between the active site and probe is less than 1 mm in the high heat flux region. In this region, frequency suddenly increases because of bubbles being emitted from the numerous active nucleation sites on the heating surface getting in touch with tip of probe. Therefore, when the probe is lowered further in the macro-layer region, it encounters the bubbles that come from the other active nucleate sites and hence the bubble emission frequency increases with decrease in height. The straight line BC represents the bubble frequency in the macro-layer region. This transition point, B, is the point of intersection obtained by extrapolating the lines AB and BC. Figure 10(b) shows the point of intersection of these two lines on an enlarged scale.

The region AB represents vapor mass frequency region. The region BC represents macro-layer region and the point B is the point of transitions of two regions. Lower the point B, small thickness liquid layer have many vapor stem as shown in Figure 2. This thin liquid layer is call macro-layer. Therefore, the height of point B above the heating surface can reasonably by interpreted as initial macro-layer thickness. The constant frequency line AB represents vapor mass frequency. Hence, for run no.16, as shown in Figure 10, the vapor mass frequency is 8Hz and macro-layer thickness is 143µm. In this way, the macro-layer thickness and vapor mass frequency at different heat fluxes (runs) were measured. Therefore, the nucleate boiling at high heat flux is characterized by the existence of a liquid layer known as the macro-layer between the heating surface and the vapor mass.

The variation of initial macro-layer thickness with respect to various heat fluxes for water boiling on brass surface at one atmospheric pressure is shown in Figure 11(a). The initial macro-layer thickness for water was found to lie in the range of 298 to 102 µm for range of heat flux 0.3 -1.1 MW/m^2. The above graph shows that the initial macro-layer thickness decreases with the increase of heat flux presumably, due to coalescence of vapor-stem occurring closer to heated wall surface as a result of increased site density of vapor-stems as heat flux is increased. Based on experimental data, the initial macro-layer was correlated as:

$$\delta_o = -263.9q + 374.1 \quad (2)$$

where, δ_o is vapor mass frequency in μm and q is heat flux in MW/m^2.

The variation of frequency of vapor mass with respect to heat flux is shown in Figure 12. The vapor mass frequency at a given heat flux was determined by taking the average of five measurements during the downward travel of the probe at many locations in the vertical plane that was sufficiently above the macro-layer at boiling surface. It was observed that the frequency of vapor mass increased with the increase in heat flux. It varied from 4 Hz to 8.8 Hz for heat flux range of 0.3 to1.1 MW/m^2 of water boiling on brass surface at one atmospheric pressure. The increase in the vapor mass frequency with the heat flux can be attributed to the higher evaporation rate associated with higher heat flux condition. Based on the above data, the vapor mass frequency was correlated with heat flux as:

$$f_v = 1.8q + 3.8 \quad \text{for} \left(0.3 \le q \le 0.9\right) \tag{4}$$

$$f_v = 17.8q - 11.58 \quad \text{for} \left(0.9 < q \le 1.1\right) \tag{5}$$

Figure 13 show plots of heat flux (q) versus wall superheat ($\Delta T=T_w-T_s$) for water boiling at atmospheric pressure. The high heat flux ranging is from the 60% of critical heat flux value (QCR); also, the slope of boiling curve was found to be almost constant but differs from the low heat flux region. In this region, the individual bubbles coalesce due to very high bubble site density and form vapor mass entrapping a relatively thicker film of liquid know as macro-layer. As high pressure needs to be maintained inside the vapor mass during the growth period in order to displace the surrounding liquid, liquid cannot be supplied to the macro-layer from the surrounding when the vapor mass grows. Liquid is drawn only when the vapor mass departs. Heat is transferred from the superheated solid surface to the vapor mass mainly through the macro-layer by conduction. As the heat flux increases, the thickness of macrolayer decreases. Hence, thermal resistance offered by macrolayer thickness decreases as degree of superheat increases. The heat flux was correlated as:

$$q = -0.006(T_w - T_s)^2 + 0.343(T_w - T_s) - 3.210 \tag{3}$$

5. SUMMARY AND CONCLUSIONS

An experimental setup was designed and fabricated for the measurement of wall heat flux, wall superheat, initial macro-layer thickness and vapor mass frequency. Experiments were conducted on water, which clearly showed macro-layer formation on heated surface. The two regions of nucleate pool boiling i.e. low heat flux region and high heat flux region can be clearly distinguished. The high heat flux ranging from 60% of critical heat flux value (qcr) to critical value is characterized by the formation of macro-layer and large billowing vapor mass over it. In this region the slope of boiling curve is found to be almost constant but differs from the low heat flux region. A liquid layer entrapped between heating surface and vapor mass is called macro-layer. The maximum thickness of the macro-layer at the time of initiation of vapor mass is termed as the initial macro-layer thickness. Since a high pressure needs to be maintained inside the vapor mass during the growth period in order to work to displace the surrounding liquid, liquid cannot be supplied to the macro-layer from the surrounding when the vapor mass grows. Liquid is drawn only when the vapor mass departs. Heat is transferred from the superheated solid surface to the vapor mass mainly through the macro-layer by conduction.

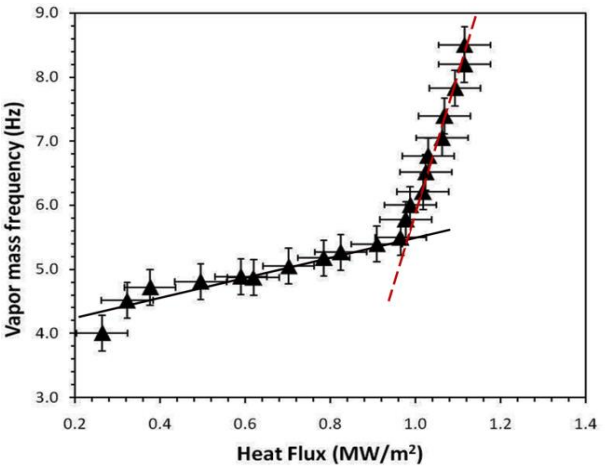

Figure 12. Vapor mass frequency (Hz) versus wall heat flux (MW/m^2). Distilled water was boiled on brass surface at room temperature 32 ^{o}C and pressure was equal to one atm. The critical point for this boiling surface is $\approx$1.15 MW/m^2.

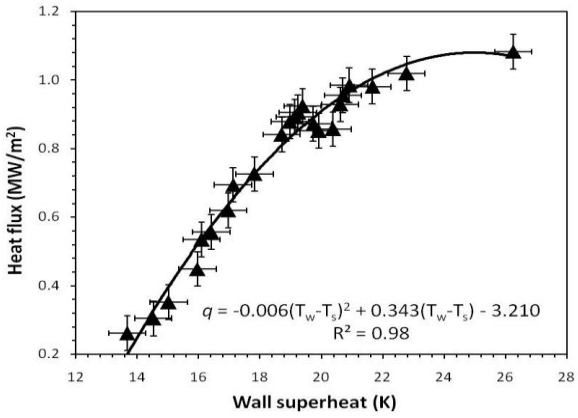

Figure 13. Heat flux (MW/m^2) versus wall super heat (K)

The heat flow rate is therefore controlled by the initial thickness of macro-layer and its thinning rate; both these parameters strongly depend upon the boiling conditions. Thus the initial macro-layer thickness is an important parameter to be determined. The initial macro-layer thickness for water was found to lay in the range of 153 to 88 μm, respectively, as the heat flux is increased from 60% of critical heat flux value to near critical value. As the heat flux increases, the thickness of initial macro-layer decreases because an increase in heat flux brings about the coalescence of vapor-stems closer to heated wall surface due to increased site density of vapor-stems. The vapor mass frequency varied from 4 to 8.80 Hz for water in this range of 60 % of critical heat flux to near critical heat value. The vapor mass frequency increases as heat flux increases due to higher evaporation rate associated with higher heat flux.

6. ACKNOWLEDGMENT

BS acknowledges to Mr. Kuldeep Lamba and Naveent Kumar Chaudhary for assisting in improving the quality of manuscript. BS is also grateful to his alma matter IITR, India for providing necessary facility to conduct the experiment.

7. REFERENCES

1. Carey, V.P., "Liquid-vapor phase-change phenomena", 2nd ed., Hemisphere Publishing Corp., New York, (1992). 342-351.
2. Diao, Y., Li, C., Zhao, Y., Liu, Y. and Wang, S., "Experimental investigation on the pool boiling characteristics and critical heat flux of cu-r141b nanorefrigerant under atmospheric pressure", ***International Journal of Heat and Mass Transfer***, Vol. 89, (2015), 110-115.
3. Fazel, S.A., Safekordi, A. and Jamialahmadi, M., "Pool boiling heat transfer in water/amines solutions", ***International Journal of Engineering***, Vol. 21, No. 2, (2008), 113-130.
4. Chung, J., Chen, T. and Maroo, S., "A review of recent progress on nano/micro scale nucleate boiling fundamentals", ***Frontiers in Heat and Mass Transfer (FHMT)***, Vol. 2, No. 2, (2011), 1-19.
5. Kim, J., "Review of nucleate pool boiling bubble heat transfer mechanisms", ***International Journal of Multiphase Flow***, Vol. 35, No. 12, (2009), 1067-1076.
6. Noie, S., Kalaei, M. and Khoshnoodi, M., "Experimental investigation of boiling and condensation heat transfer of a two phase closed thermosyphon", ***International Journal of Engineering***, Vol. 18, No. 1, (2005), 37-43.
7. Islam, M.S., Haque, K.T. and Saha, S.C., "An experimental investigation of pool boiling at atmospheric pressure", ***Daffodil International University Journal of Science and Technology***, Vol. 6, No. 1, (2011), 80-86.
8. Hameed, M.S., Khan, A.R. and Mahdi, A., "Modeling a general equation for pool boiling heat transfer", ***Advances in Chemical Engineering and Science***, Vol. 3, No. 04, (2013), 294.
9. Kandlikar, S.G., "A theoretical model to predict pool boiling chf incorporating effects of contact angle and orientation", ***Journal of Heat Transfer***, Vol. 123, No. 6, (2001), 1071-1079.
10. He, Y., Shoji, M. and Maruyama, S., "Numerical study of high heat flux pool boiling heat transfer", ***International Journal of Heat and Mass Transfer***, Vol. 44, No. 12, (2001), 2357-2373.
11. Gaertner, R., "Photographic study of nucleate pool boiling on a horizontal surface", ***Journal of Heat Transfer***, Vol. 87, No. 1, (1965), 17-27.
12. Bhat, A., Prakash, R.t. and Saini, J., "On the mechanism of macrolayer formation in nucleate pool boiling at high heat flux", ***International Journal of Heat and Mass Transfer***, Vol. 26, No. 5, (1983), 735-740.
13. Bhat, A., Prakash, R. and Saini, J., "Heat transfer in nucleate pool boiling at high heat flux", ***International Journal of Heat and Mass Transfer***, Vol. 26, No. 6, (1983), 833-840.
14. Kirby, D. and Westwater, J., "Bubble and vapor behavior on a heated horizontal plate during pool boiling near burnout", in Chem. Eng. Prog., Symp. Ser. Vol. 61, (1965), 238-248.
15. Ahn, H.S. and Kim, M.H., "Visualization study of critical heat flux mechanism on a small and horizontal copper heater", ***International Journal of Multiphase Flow***, Vol. 41, (2012), 1-12.
16. Chyu, M.-C., "Evaporation of macrolayer in nucleate boiling near burnout", ***International Journal of Heat and Mass Transfer***, Vol. 30, No. 7, (1987), 1531-1538.
17. Iida, Y. and Kobayasi, K., "Distributions of void fraction above a horizontal heating surface in pool boiling", ***Bulletin of JSME***, Vol. 12, No. 50, (1969), 283-290.
18. Wei, J., Yu, B. and Wang, H., "Heat transfer mechanisms in vapor mushroom region of saturated nucleate pool boiling", ***International Journal of Heat and Fluid Flow***, Vol. 24, No. 2, (2003), 210-222.
19. Nishio, S., Gotoh, T. and Nagai, N., "Observation of boiling structures in high heat-flux boiling", ***International Journal of Heat and Mass Transfer***, Vol. 41, No. 21, (1998), 3191-3201.
20. Sadasivan, P., Chappidi, P., Unal, C. and Nelson, R., "Possible mechanisms of macrolayer formation", ***International Communications in Heat and Mass Transfer***, Vol. 19, No. 6, (1992), 801-815.
21. Katto, Y. and Yokoya, S., "Principal mechanism of boiling crisis in pool boiling", ***International Journal of Heat and Mass Transfer***, Vol. 11, No. 6, (1968), 993-1002.
22. Bhat, A., Saini, J. and Prakash, R., "Role of macrolayer evaporation in pool boiling at high heat flux", ***International Journal of Heat and Mass Transfer***, Vol. 29, No. 12, (1986), 1953-1961.
23. Ono, A. and Sakashita, H., "Liquid–vapor structure near heating surface at high heat flux in subcooled pool boiling", ***International Journal of Heat and Mass Transfer***, Vol. 50, No. 17, (2007), 3481-3489.
24. Sakashita, H. and Ono, A., "Boiling behaviors and critical heat flux on a horizontal plate in saturated pool boiling of water at high pressures", ***International Journal of Heat and Mass Transfer***, Vol. 52, No. 3, (2009), 744-750.
25. Sakashita, H., Ono, A. and Nakabayashi, Y., "Measurements of critical heat flux and liquid–vapor structure near the heating surface in pool boiling of 2-propanol/water mixtures", ***International Journal of Heat and Mass Transfer***, Vol. 53, No. 7, (2010), 1554-1562.
26. Ohta, H., "Experiments on microgravity boiling heat transfer by using transparent heaters", ***Nuclear Engineering and Design***, Vol. 175, No. 1, (1997), 167-180.

27. Rajvanshi, A., Saini, J. and Prakash, R., "Investigation of macrolayer thickness in nucleate pool boiling at high heat flux", ***International Journal of Heat and Mass Transfer***, Vol. 35, No. 2, (1992), 343-350.

Experimental Study for Investigating the Mechanism of Heat Transfer near the Critical Heat Flux in Nucleate Pool Boiling

B. S. Sikarwar, R .K. Shukla, S. K. Sharma

Amity School of Engineering Technology, Amity University Noida (UP), India

P A P E R I N F O

Paper history:
Received 15 April 2015
Received in revised form 05 June 2015
Accepted 12 June 2015

Keywords:
Pool Boiling Nucleate
Macro-layer
Mashroom
Critical Heat Flux
Vapor Mass
Frequency

چکیده

رژیم هسته استخر جوش در نزدیکی شار حرارتی بحرانی (CHF 60-98٪) به عنوان رژیم قارچ بخار شناخته شده است . درک مکانیسم انتقال حرارت در رژیم قارچ بخار هسته استخر جوش نه تنها برای توضیح نرخ انتقال حرارت بالا مفید است، بلکه برای توضیح پدیده بحران جوش نیز سودمند است. در این مقاله، یک سیستم آزمایشگاهی طراحی و ساخته شد تا مکانیسم انتقال حرارت از سطح جوش به توده مایع نزدیک شار حرارتی بحرانی (رژیم قارچ بخار) مطالعه شود. علاوه بر این، فرکانس توده بخار و ضخامت لایه ماکرو در شارهای حرارتی مختلف در این رژیم جوش اندازه گیری شد. مطالعه تجربی نشان می دهد که حباب های تکی با توجه به چگالی سایت بسیار بالای حباب به هم می چسبند و توده بخار تشکیل می دهند که در یک فیلم نسبتا ضخیم تر از مایع محبوس می شوند که به عنوان ماکرو–لایه شناخته شده و بین جرم بخار در حال رشد و سطح گرمایش استخر جوش در نزدیکی منطقه شار حرارتی بالا است. میزان تبخیر آب از لایه ماکرو و هدایت گذرا از طریق ماکرو لایه پارامتر نخست برای انتقال حرارت از سطح گرم است. ضخامت لایه های ماکرو در محدوده 153– 88 میکرومتر، به ترتیب، برای طیف وسیعی از 60–98٪ شار حرارتی بحرانی است. هنگامی که شار گرما افزایش می یابد، ضخامت لایه ماکرو کاهش می یابد. فرکانس توده بخار از 4 هرتز تا 8.80 هرتز برای آب در محدوده 60–98٪ شار حرارتی بحرانی متفاوت است. فرکانس توده بخار جرم با افزایش شار گرما افزایش می دهد که این امر به دلیل میزان تبخیر بالاتر در ارتباط با شار حرارتی بالاتر است. داده های گزارش شده در این مقاله نسبت به داده های موجود در متون سازگارتر هستند و این داده ها در مدل سازی انتقال حرارت در هسته استخر جوش در نزدیکی شار حرارتی بحرانی مفید واقع می شوند.

***doi**: 10.5829/idosi.ije.2015.28.08b.18*